Charging and $E\times B$ rotation of ablation clouds surrounding refueling pellets in hot fusion plasmas

P. B. Parks,[1] T. Lu,[2] and R. Samulyak[2]
[1]*General Atomics, P.O. Box 85608, San Diego, California 92186-5608, USA*
[2]*Computational Science Center, Brookhaven National Laboratory, Upton, New York 11973, USA*

(Received 10 March 2009; accepted 2 June 2009; published online 26 June 2009)

The finite resistivity magnetohydrodynamic code FRONTIER-MHD [R. Samulyak *et al.*, Nucl. Fusion **47**, 103 (2007)] is used to simulate the ablation rate of refueling pellets, including the novel effect of electrostatically induced $E\times B$ rotation of the ablation cloud about its symmetry axis parallel to the magnetic field. The key finding is that the centrifugal force of cloud rotation pushes the cloud density radially outwards, creating a more "transparent" ablation channel. With reduced shielding, the *steady state* ablation rate of a deuterium pellet significantly increases from ~35% to 100%, depending on the B-field strength. This new effect brings the ablation rate into better accord with a known theoretical scaling law, which agrees with most current experiments. © *2009 American Institute of Physics*. [DOI: 10.1063/1.3158562]

In the last 30 years a large body of literature has been devoted to the study of hydrogenic pellet injection for fueling magnetically confined devices.[1] Pellet fueling could enable tokamak operation at higher central densities above the Greenwald limit needed for achieving greater fusion power in reactor scale devices such as ITER.[2] The deposition of the fuel within plasma is quite complex and involves two process, pellet disassembly by ablation and subsequent redistribution of the freshly ionized material down the magnetic field gradient by the toroidally induced grad-B drift effect.[3,4] Standard one-dimensional spherically symmetric, quasisteady ablation models provide convenient scaling laws and predict with good success pellet penetration depth in current devices. However, lacking comprehensive two- (2D) and three-dimensional (3D) magnetohydrodynamic (MHD), time-dependent, and electrostatic charging effects, predicting fuel deposition profiles in high-temperature, high-magnetic field ITER class devices remains uncertain. When a pellet is immersed in hot plasma, it ablates and forms a cold, dense vapor cloud around it. Under the force of its own pressure, the neutral cloud expands almost isotropically until it becomes sufficiently heated and ionized downstream by the incoming "drive" electrons following tight helical trajectories around magnetic field lines. The magnetic field acting through the $J\times B$ force then impedes the outflow in the cross-field direction while expanding freely in the parallel (magnetic field) direction, forming an elongated weakly diamagnetic field-aligned structure (ionized ablation channel). The higher line density of the nearly 1D ablation channel enhances interception and absorption of the energy flux carried to the pellet thus regulating the ablation rate. The pressure, density, and width of the ablation column are essential for predicting the subsequent grad-B drift rate.[4] The extra longitudinal line density (opacity) of the ablation column also enhances interception and absorption of the energy flux carried to the pellet, as verified by recent 2D MHD simulations of pellet ablation.[5] Depending on the magnetic field strength and the energy flux rise time seen by a (moving) pellet, the ablation rate can be slowed by factors of ~3.

This result, however, underpredicts the ablation rate by factors of 2-ish compared to experimental measurements in current tokamak plasmas with typical fields $B\sim 2$ T. In the present letter, we show that the discrepancy can be removed by self-consistently including $E\times B$ rotation of the ablation column about its symmetry axis parallel to B. The radial electric field E inside the cloud comes about because the cloud charges negatively with respect to the background plasma to equalize electron and ion particle currents at opposite end face boundaries, Fig. 1(a). Quasineutrality in the background plasma confines the main electric potential difference $-\phi_s(>0)$ to a thin collisionless sheath at each end face. (Various charging models were summarized in the excellent review article by Pegourie.[1]) Since the longitudinal opacity of the ablation column to the incident electrons decreases radially outward,[5] a radial variation in $-\phi_s$ develops, giving rise to a radial electric field and $E\times B$ rotation. The outward centrifugal force of rotation widens the ablation channel and reduces line density. Accordingly, pellet shielding is weakened and the ablation rate increases.

Figure 1(b) illustrates the various particle fluxes entering, exiting, or being emitted from the right cloud/plasma interfacial sheath. The cold and dense ablation channel stops the short-range plasma ion flux, given by $\Gamma_{\|i}\cong 0.55 n_{i\infty}(T_{e\infty}/m_i)^{1/2}$ (Ref. 6). The incident electron flux $\Gamma_{\|e\infty}=n_{e\infty}(T_{e\infty}/2\pi m_{e\infty})^{1/2}$ is electrostatically repelled, giving rise to passing electrons with reduced particle flux $\Gamma_{\|ep}=\Gamma_{\|e\infty}e^{-\Phi_s}$ on both sides of the sheath (reflected electrons obviously do not contribute to the net flux), $\Gamma_{\|ec}=\Gamma_{\|e\infty}(1-\mu_s)\sqrt{\pi\Phi_s}\,\mathrm{erfc}(\sqrt{\Phi_s})$ is the outward flux of cold cloud electrons after being accelerated across the sheath, and the symbol "∞" refers to any ambient plasma parameter, and $\Phi_s=-\phi_s/T_{e\infty}(\mathrm{eV})$. The collisionally attenuated flux of right going hot plasma electrons that traversed the full length of the cloud after entering it from the left end face is $\Gamma_{\|ea}=\mu_s\Gamma_{\|ep}$, with attenuation coefficient $\mu_s(\tau_*)$ $(0<\mu_s<1)$, depending on the radially varying cloud opacity $\tau_*(r)=\int_{-\infty}^{\infty}n(r,z')dz'$. From the same kinetic electron model used before to obtain the attenuated energy flux,[4,7] we find that

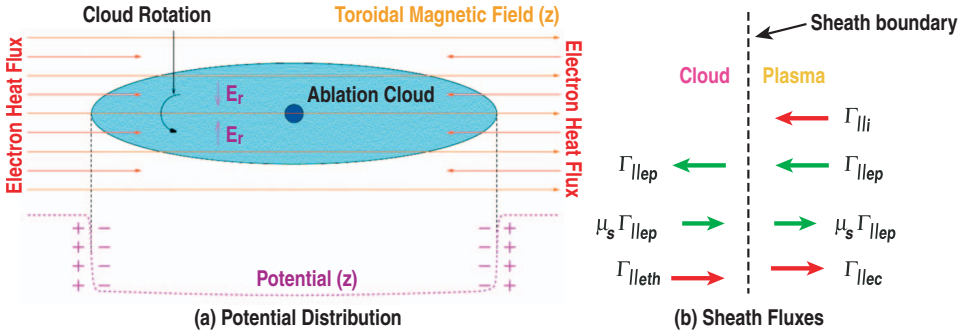

FIG. 1. (Color) Various charged particle fluxes entering/exiting the cloud-plasma sheath.

$$\mu_s(u_*) = \left[1 + \left(\frac{u_*}{2}\right)^{1/2} - \frac{u_*}{4} + \frac{1}{2}\left(\frac{u_*}{2}\right)^{3/2}\right]\exp[-(u_*/2)^{1/2}] - \frac{u_*^2}{8}E_1[(u_*/2)^{1/2}],$$

where $u_* = \tau_*(r,z)/\tau_\infty$, $\tau_\infty = T_{e\infty}^2/8\pi e^4 \ln\Lambda$, and $E_1(z)$ is the exponential integral. Hence the steady-state ambipolarity condition, $\Gamma_{\|i}+\Gamma_{\|ec}-\Gamma_{\|ep}(1-\mu_s)=0$, leads to an implicit expression for the normalized sheath potential, $\exp(-\Phi_s) - \sqrt{\pi\Phi_s}\,\mathrm{erfc}(\sqrt{\Phi_s}) = \alpha/(1-\mu_s)$,[6] also having a radial variation, where $\alpha = 0.55(2\pi m_e/m_i)^{1/2}$. To estimate the radial electric field E_r, we can neglect the weak longitudinal z variation in the potential $\phi(r,z)$. Therefore, $E_r = -\partial\phi/\partial r \cong T_{e\infty}(d\Phi_s/d\mu_s)(d\mu_s/du_*)(du_*/dr)$. Consider now a D_2 pellet with $r_p = 2$ mm, $T_{e\infty} = 2000$ eV, $n_{e\infty} = 10^{14}$ cm^{-3}, and $B = 6$ T. Using results from previous simulations without rotation,[5] we find at radius $r = 1.29$ cm from symmetry axis that $\tau_* = 6.03\times10^{18}$ cm^{-2}, $u_* = 7.85$, $du_*/dr = -49.5$ cm^{-1}, $\mu_s = 0.2899$, $\Phi_s = 1.697$, and $E_r = -0.31$ MV/m. The rotation velocity $u_\theta = -E_r/B_z = 52$ km/s can indeed become supersonic for a ~ 5 eV cloud temperature.

The 2D finite-resistivity FRONTIER-MHD code[5] is used to model the charging/rotation problem using a cylindrical system of coordinates (r,θ,z) with axisymmetry $\partial/\partial\theta = 0$. The key assumption is that the ablation flow is either sufficiently resistive or else weakly diamagnetic, so that a static magnetic field can be assumed, $\boldsymbol{B} = B\hat{z}$, as will be confirmed *a posteriori*. The governing equations are essentially the same as before,[5] with the exception of the two transverse-to-B components of the momentum equation that include azimuthal rotation,

$$\rho\left(\frac{\partial u_r}{\partial t} + u_r\frac{\partial u_r}{\partial r} + u_z\frac{\partial u_r}{\partial z}\right) + \frac{\partial p}{\partial r} = J_\theta B + \rho\frac{u_\theta^2}{r}, \tag{1}$$

$$\rho\left(\frac{\partial u_\theta}{\partial t} + u_r\frac{\partial u_\theta}{\partial r} + u_z\frac{\partial u_\theta}{\partial z}\right) = -J_r B - \rho\frac{u_r u_\theta}{r}, \tag{2}$$

where $\boldsymbol{u}$, $\rho = m_i n$, and p are, respectively, the velocity, mass density, and pressure of the ablation cloud. The total current density is $\boldsymbol{J}_{\rm tot} = \boldsymbol{J} + J_h\hat{z}$, where $J_h = -e(\mu_+ - \mu_-)\Gamma_{\|ep}$ is the hot electron current density in the cloud with $\mu_\pm$ being the local particle attenuation coefficients for right (+) and left (−) going particle fluxes. Ohm's law provides the following components of the thermal electron current density $\boldsymbol{J}$: $J_r = -\sigma_\perp(-\partial\phi/\partial r + u_\theta B)$, $J_\theta = -\sigma_\perp u_r B$, and $J_z \equiv -e\Gamma_{\|eth} = -\sigma_\|\partial\phi/\partial z$. The parallel (perpendicular) electrical conductivities, $\sigma_\|(\sigma_\perp)$, are given by a convenient "addition rule": $\sigma_\| = n_e e^2/m_e(0.506\nu_{ei} + \nu_{eg} + \nu_{ea})$ and $\sigma_\perp = n_e e^2/m_e(\nu_{ei} + \nu_{eg} + \nu_{ea})$, where ν_{ei} is the e-i collision frequency, and ν_{eg}, ν_{ea} are momentum transfer collision frequencies between electrons and molecules/atoms. Imposing $\nabla\cdot\boldsymbol{J}_{\rm tot} = 0$ provides closure to the system of equations and leads to an elliptic equation for the electrostatic potential $\phi(r,z,t)$ in the body of the cloud (excluding the thin sheath region), $\partial[r\sigma_\perp(-\partial\phi/\partial r + u_\theta B)]/\partial r + r\partial(-\sigma_\|\partial\phi/\partial z + J_h)/\partial z = 0$. The boundary condition follows from the continuity of $\hat{n}\cdot\boldsymbol{J}_{\rm tot}$ across the surface of the cloud, where $\hat{n}$ is the unit surface normal vector pointing outward from the surface. Since the hot ambient plasma region is very tenuous and highly conductive, it cannot support appreciable radial polarization currents as compared to the denser and more collisional cloud region. Consequently, on the plasma side of the interface $J_{r,\rm out} = 0$, which formally leads to a surface boundary condition, $(\hat{z}\cdot\hat{n})(\sigma_\|\partial\phi/\partial z - e\Gamma_{\|i} - e\Gamma_{\|ec}) = \sigma_\perp(\hat{r}\cdot\hat{n})(-\partial\phi/\partial r + u_\theta B_z)$. Initially, the cloud spins up to the $E\times B$ rotation velocity by means of the torque density $|\boldsymbol{r}\times(\boldsymbol{J}\times\boldsymbol{B})| = rBJ_r$, resulting from a transient radial polarization current flow J_r. From Eq. (2) and Ohm's law, the estimated time scale for spin up is $\tau_s = \rho/(\sigma_\perp B^2) = \tau_A/S \sim 0.01-0.05$ μs, where $\tau_A = r_\perp/V_A$ is the characteristic Alfvén time scale, and $S = \mu_0\sigma_\perp r_\perp V_A$ is a dimensionless Lundquist number, typically $S\sim 15$. Since the time scale for evolution of the ablation cloud is much longer, $\sim 1-10$ μs, we may assume that at each moment the rotational velocity equals the instantaneous value of the asymptotic $E\times B$ rotation velocity $u_\theta \cong -E_r/B_z$. In this approximation $J_r \cong 0$, so that Eq. (2) becomes superfluous. Also a simplified potential equation follows: $-\sigma_\|\partial\phi/\partial z + J_h = (-\sigma_\|\partial\phi/\partial z + J_h)|_{\rm sheath} = 0$, reducing the surface boundary condition to $\sigma_\|\partial\phi/\partial z|_{\rm sheath} = e\Gamma_{\|i} + e\Gamma_{\|ec}$. By eliminating $\sigma_\|\partial\phi/\partial z|_{\rm sheath}$ between these two equations, we recover the steady-state ambipolarity condition written previously. Consequently, the normalized potential at any interior point becomes

$$\Phi(r,z) = \Phi_s(r) - T_{e\infty}^{-1}\int_z^\infty \frac{J_h(r,z')}{\sigma_\|(r,z')}dz'. \tag{3}$$

Usually thermal equilibrium is approximately maintained in the expanding outflow, so that the ionization and molecular dissociation fractions f_i and f_d can be obtained from known functions of temperature and density (Saha equations). However, in approaching the pellet surface $f_i \to 0$ and Φ blows up. With few return current carriers, a negative space charge accumulates, constituting a so-called "negative layer" (NL),

where the potential undergoes a significant drop near the pellet due an accumulation of negative charge, as will be shown. To correctly treat the potential distribution in the NL, one must account for the *extra source* of cold electrons resulting from hot electron impact ionization, giving rise to cold thermalized electrons with density $n_{es}=n_g^+ + n_a^+$ and temperature $T_e \approx T$. We can obtain the densities of molecular n_g^+ and ordinary n_a^+ ions in the NL by using improved impact ionization/recombination balance equations, obtaining $n_{es}=\chi\bar{n}$ from a root of the cubic equation $\chi^3-(1-f_d)\chi-f_d\omega=0$, where $\bar{n}=(-J_h n Q_i/2e\alpha_{DR})^{1/2}$, $\omega\equiv\alpha_{DR}/\bar{n}\alpha_3$, Q_i is the absolute electron-impact ionization cross section evaluated at energy $T_{e\infty}$, and α_{DR}, α_3 are radiative and three body recombination rates, respectively. Inserting $n_e=n_{es}+f_i n$ into $\sigma_\parallel$ prevents Φ from blowing up as $f_i\rightarrow 0$ near the pellet.

In a tokamak with major radius R, the grad-B drift curves the centroid of the ablation channel away from the z-axis or central pellet shadow. To mimic this 3D effect in a 2D model, we limit the extent of the ablation flow to a certain axial distance z_L.[4] In the following numerical simulations we choose $z_L=15$ cm and apply standard outflow boundary conditions at that point, with zero heat flux absorption for $z>z_L$.[5]

Simulations were performed using the FRONTIER-MHD code applied previously to pellet ablation with no rotation.[5] To benchmark our new results with the previous no rotation results and compare with current experiments, we consider a stationary D_2 pellet exposed to plasma with nominal reference parameters: $T_{e\infty}=2$ keV, $n_{e\infty}=10^{14}$ cm^{-3}, and $r_p=2$ mm. Since the simulation must begin by specifying the rise time t_R of the incident electron heat flux,[5] we assume here that $T_{e\infty}$ and $n_{e\infty}$ are ramped up linearly to these values over the time $t_R=10$ μs. Thereafter, the simulation proceeds until the ablation profile reaches a steady state. With rotation turned off, the ablation rates at steady state for three different values of the magnetic field strength are as follows: $G=22$ g/s for $B=2$ T, $G=19$ g/s for $B=4$ T, and $G=17$ g/s for $B=6$ T. When rotation is included, these respective ablation rates are all increased by about a factor of 2: $G=48.5$ g/s for $B=2$ T, $G=31$ g/s for $B=4$ T, and $G=26.6$ g/s for $B=6$ T. For $B=2$ T the computed ablation rate 48.5 g/s is somewhat higher ($\sim$24%) when compared with the standard quasisteady ablation model,[8] which predicts $G_{qs}=39$ g/s, which also agrees with the body of experimental data on contemporary tokamaks.[9] With no rotation, the discrepancy between G and G_{qs} is considerably higher $\sim$45%, suggesting to us that the rotation phenomenon is highly probable and represents an important improvement in 2D pellet ablation modeling. Because the penetration depth scales roughly as $\lambda_{\rm pen}\propto G^{-1/3}$, our simulation with rotation predicts a 16% increase in penetration depth when B increases from 2 to 4 T. This result is in accordance with the 17% increase in *measured* penetration depth *relative* to the penetration depth predicted by the standard models for two different machines, ASDEX ($B=2.2$ T) and Tore Supra ($B=4$ T). Furthermore, the $NGPS_R$ quasisteady model[10] (which contains an *ad hoc* B field dependence) predicts a 10% increase in the penetration depth in Tore Supra when the B field increases from 2 to 4 T. It was also found in field reversed experiment, where the B field is much lower than in standard tokamaks, that the ablation rate is 2–2.5 times higher than that predicted by the standard quasisteady ablation models.[11] Although these experiments are congruent with our numerical trends on the B scaling, recent empirical data on pellet penetration from the high-field side of ASDEX Upgrade[12] find that penetration depth has a weak *inverse* B scaling. One possible explanation could be the difficulty in isolating B variations independently from other plasma parameters.

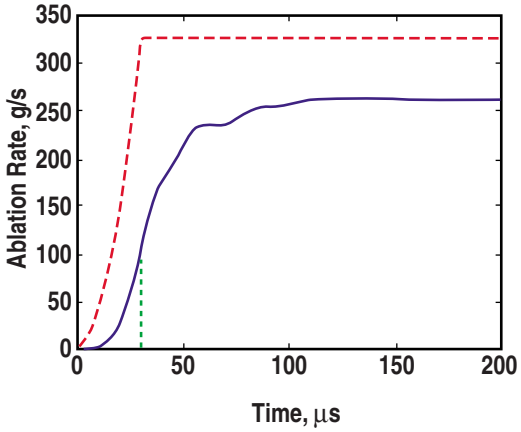

FIG. 2. (Color online) Ablation rate comparison with the quasisteady ablation models. The solid line is the ablation rate from the simulation and the dashed line is the prediction of the quasisteady ablation models. The vertical line indicates the end of plasma warm up in the pedestal region.

Next, we consider the ablation rate of a moving pellet. The pellet is injected into an ITER H-mode plasma discharge,[2] with initial pellet radius $r_p=4$ and velocity $V=3$ km/s based on a newly proposed high-velocity pellet injection concept using gyrotron power.[13] The pellet first crosses the edge-pedestal layer with steep plasma profiles, which we assume to be linear from the plasma boundary up to the top of pedestal, over the range $0.2\ \text{keV}\leq T_{e\infty}\leq 4$ keV and $2\times 10^{13}\ \text{cm}^{-3}\leq n_{e\infty}\leq 10^{14}\ \text{cm}^{-3}$, with flat profiles beyond.[2] The pedestal width is assumed to be $\Delta_{\rm ped}=9$ cm, so that the heat flux rise time along the pellet trajectory is effectively, $t_R=\Delta_{\rm ped}/V=30$ μs. Figure 2 shows that the *transient* ablation rate dramatically lags behind the faster rising quasisteady ablation rate G_{qs} by about a factor of 3. Since the pedestal suffers intermittent collapse from ELMs,[2] having decreased ablation in the pedestal region would most likely result in more efficient utilization of the (tritium) fuel for sustained fusion power generation. Both models, however, are in fairly close agreement when steady state is finally approached: $G=262$ g/s, which is only 20% lower than $G_{qs}=327$ reached at the pedestal top. With rotation turned off, G approaches a lower steady state value of 195 g/s, 40% lower than G_{qs}.

Figure 3 plots the Mach number of the rotational velocity $M_\theta=u_\theta/c_s$ when the flow reaches a quasisteady state. It has a transonic distribution and sonic points are located in the ablation channel at $r_{\rm rot}^*\cong 6r_p$. The centrifugal force of rotation widened the ablation channel and reduced the density near the axis, as seen in Fig. 4 where we compare 2D images of pressure and density contours with and without rotation when a steady state is reached. The channel bound-

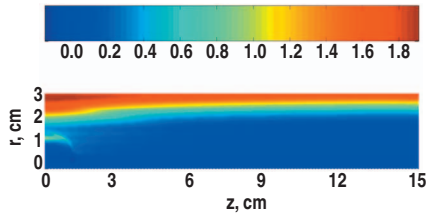

FIG. 3. (Color) Rotational Mach number distribution in the steady-state ablation cloud.

ary r_c is defined as the radial location of the steepest pressure gradient. The normalized channel radius $\kappa_c = r_c/r_p$, a key nondimensional parameter in pellet drift models,[4] increased from $\kappa_c = 5.75$ without cloud rotation to $\kappa_c = 8$ with rotation. The cloud pressure distribution along the z-axis was only reduced by 7% from the no rotation case because of the compensating higher temperature: pressure decreased monotonically from 25 bars at the "entrance" of elongated section of the ionized ablation channel, $z \sim 7$ mm, to 10 bars at the sonic $(M=1)$ "exit" plane $z \sim z_L$. The cloud beta $\beta = 2\mu_0 p/B^2$ characterized by the channel entrance value is therefore $\beta = 0.17$, indicating that the level of diamagnetism $|\Delta B/B| \cong \beta/2 = 0.087$ is small enough to justify the assumption of a static B field.

The distribution of the normalized electrical potential Φ along different field lines (Fig. 5) shows that the potential drop in the NL is about 700 V, which is relatively small compared with the ~7840 V sheath potential drop. As a result, the potential and radial electric field is essentially determined by the first term in Eq. (3). Notice that E_r and thus the rotation is larger toward the boundary of the ablation channel and explains the edge-peaked M_θ distribution in Fig. 3.

In conclusion, the electrostatic charging and rotation of magnetized pellet ablation clouds has included self-consistently in the 2D FRONTIER-MHD code. We have shown that the outward centrifugal force of cloud rotation widens the long ionized ablation cylinder, and the accompanying density rarefaction reduces the shielding of the pellet by the incoming plasma heat flux. As a result, the ablation rate is increased by factors of 2. This result is noteworthy, because the steady-state ablation rate now concurs with the pellet

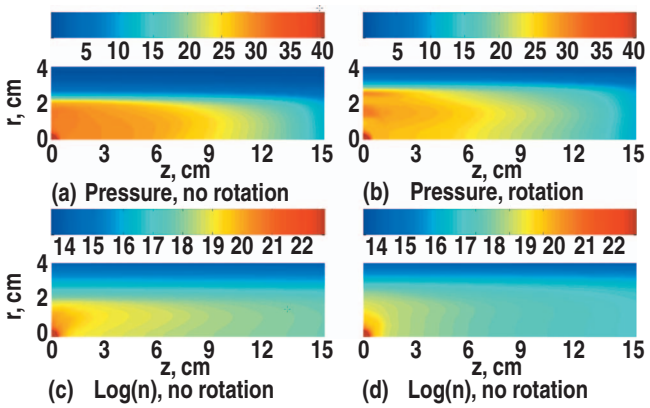

FIG. 4. (Color) Steady-state ablation flows showing contours of pressure and density with and without rotation.

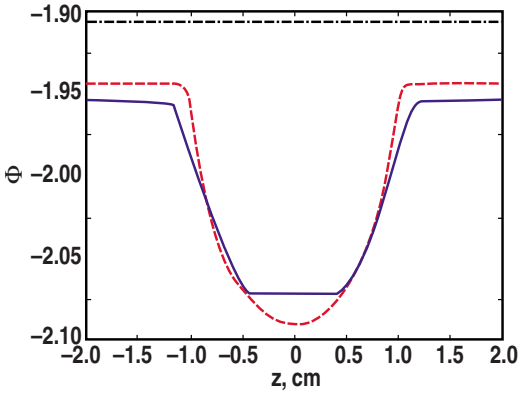

FIG. 5. (Color online) Normalized electrical potential distribution in steady-state ITER case. The solid line is along z-axis, the dashed line is along $r = 2r_p$, and the dotted line is along $r = 4r_p$, where $r_p = 4$ mm is the pellet radius for ITER case.

injection experiments on existing devices. All currently used ablation models and scaling laws are essentially quasisteady, 1D spherically symmetric, and physically limited due to a lack MHD and rotation effects. Hence, their agreement with the experiments (with possibly adjusted ablation coefficients in some cases) is merely fortuitous. It seems to us that a reasonable interpretation for finding that $G < G_{qs}$ in the ITER $B=6$ T case, as opposed to $G > G_{qs}$ in the $B=2$ T current machine case, is because a stronger B-field promotes better channel shielding by creating a more narrow and dense ablation channel, which rotates with lower $E \times B$ velocity, $u_\theta = E_r/B$.

This work was supported by the U.S. Department of Energy under Grant Nos. DE-AC02-98CH10886, with Brookhaven Science Associates, LLC, and DE-FG03-95ER54309 with General Atomics. This research partially used resources of the National Energy Research Scientific Computing Center, which is supported by the Office of Science of the U.S. Department of Energy under Contract No. DE-AC03-76SF00098.

[1] B. Pegourie, Plasma Phys. Controlled Fusion **49**, R87 (2007).
[2] M. Shimada, D. J. Campbell, V. Mukhovatov, M. Fujiwara, N. Kirneva, K. Lackner, M. Nagami, V. D. Pustovitov, N. Uckan, and J. Wesley, Nucl. Fusion **47**, S1 (2007).
[3] B. Pegourie, V. Waller, H. Nehme, L. Garzotti, and A. Geraud, Nucl. Fusion **47**, 44 (2007).
[4] P. B. Parks and L. R. Baylor, Phys. Rev. Lett. **94**, 125002 (2005); P. B. Parks, W. D. Sessions, and L. R. Baylor, Phys. Plasmas **7**, 1968 (2000).
[5] R. Samulyak, T. Lu, and P. Parks, Nucl. Fusion **47**, 103 (2007).
[6] P. B. Parks, Plasma Phys. Controlled Fusion **38**, 571 (1996).
[7] R. Ishizaki, P. B. Parks, N. Nakajima, and M. Okamoto, Phys. Plasmas **11**, 4064 (2004).
[8] P. B. Parks and M. N. Rosenbluth, Phys. Plasmas **5**, 1380 (1998).
[9] L. R. Baylor, A. Geraud, W. A. Houlberg, D. Frigione, M. Gadeberg, T. C. Jernigan, J. De Kloe, P. Kupschus, B. V. Kuteev, P. Lang, A. A. M. Oomens, A. L. Qualls, K. N. Sato, and G. L. Schmidt, Nucl. Fusion **37**, 445 (1997).
[10] B. Pegourie, J.-M. Picchiottino, H.-W. Drawin, A. Geraud, and M. Chatelier, Nucl. Fusion **33**, 591 (1993).
[11] A. Canton, B. Pegourie, and P. Innocente, Plasma Phys. Controlled Fusion **43**, 225 (2001).
[12] E. Belonohy, O. J. W. F. Kardaun, T. Feher, K. Gal, S. Kalvin *et al.*, Nucl. Fusion **48**, 065009 (2008).
[13] P. B. Parks and F. W. Perkins, Nucl. Fusion **46**, 770 (2006).